An Open-Source Framework for IEEE 802.11bf Evaluation Under Lossy and Jittery Conditions

Tanguy Ropitault*,†, Steve Blandino*,†, Nada Golmie‡
*Associates, CTL, National Institute of Standards and Technology, Gaithersburg, MD, USA
†Prometheus Computing LLC, Bethesda, MD, USA
‡CTL, National Institute of Standards and Technology, Gaithersburg, MD, USA

Email: {tanguy.ropitault, steve.blandino, nada.golmie}@nist.gov

***Abstract*—Integrated Sensing and Communication (ISAC) is emerging as a key enabler for future wireless systems, offering dual communication and sensing capabilities using the same hardware. A leading realization of this paradigm is Wi-Fi sensing, now being standardized in IEEE 802.11bf, which expands Wi-Fi's role into environmental awareness. Wi-Fi sensing can support diverse applications, from smart homes to healthcare, and is highly relevant for military and security use, enabling intrusion detection, silent perimeter monitoring, and situational awareness, without dedicated radar infrastructure. However, like conventional IEEE 802.11 networks, 802.11bf sensing is prone to delays and losses from contention-based access, interference, collisions, and congestion. These issues can significantly degrade sensing, which relies on consistently timed and complete measurements.**

This paper presents an extension of the open-source ISAC-Physical Layer Model (PLM) framework to enable the evaluation of Wi-Fi sensing under lossy and irregular timing. In an indoor military surveillance scenario, results show that velocity accuracy significantly degrades with the packet loss and timing irregularities. These findings highlight the need for resilient sensing algorithms and robust, reproducible testing environments, both of which being supported by our proposed platform.

***Index Terms*—IEEE 802.11bf, ISAC, Open-Source.**

I. Introduction

Wireless sensing leverages communication devices as sensors, enabling them to extract environmental information by analyzing subtle variations in radio signals reflected off objects and individuals. This dual-functionality aligns with the broader vision of *Integrated Sensing and Communication* (ISAC), which aims to unify sensing and communication within a shared infrastructure. Wireless sensing supports a diverse set of applications, including intrusion detection in smart homes, gesture recognition and HVAC automation in smart buildings, and vital sign monitoring in healthcare [1].

In military and homeland security contexts, Wi-Fi sensing is especially valuable, offering a stealthy alternative to traditional sensing systems such as radar. By leveraging existing communication infrastructure, wireless sensing enables covert environmental awareness without requiring additional hardware, an advantage when constraints on power, space, or operational discretion exist. Furthermore, unlike conventional sensors that often depend on line-of-sight, wireless sensing can function effectively in obstructed environments, such as through smoke, low light, or even walls, making it particularly well-suited for conditions where visibility is limited or unpredictable. For instance, forward-deployed military units or mobile command centers utilizing Wi-Fi for communication can repurpose those same signals for motion detection or activity recognition, enhancing situational awareness at no additional radio frequency (RF) cost. Likewise, stationary deployments such as base perimeters, embassies, or secure facilities can benefit from passive monitoring of internal spaces and passageways.

These operational scenarios highlight the relevance of the upcoming IEEE 802.11bf standard, scheduled for finalization in 2025, which formalizes Wi-Fi sensing capabilities across both sub-7 GHz and high-resolution millimeter waves (mmWave) Directional Multi-Gigabit (DMG) bands [2]. These are referred to respectively as the *sensing procedure* and the *DMG sensing procedure*, the latter being the focus of this paper as it provides better resolution, up to the centimeter level. Performing effective sensing requires regularly spaced and reliable measurements to accurately interpret environmental changes. However, real-world wireless deployments often feature irregular traffic patterns, contention-based channel access, interference, limited resources and coordination, and mobility-induced variability. As demonstrated in recent studies [3], these conditions produce irregular and lossy sensing intervals, which significantly impair sensing performance and form a Lossy and Irregular Timing Sensing System (LITSys).

Radar systems have addressed similar challenges by leveraging *compressed sensing* (CS), exploiting signal sparsity to reconstruct information from fewer samples than traditional methods [4], [5]. Recently, CS principles have been effectively extended to Wi-Fi sensing. Pegoraro et al.'s SPArse Recovery Approach for Integrated Communication and human Sensing (SPARCS) approach recovers micro-Doppler signatures from sparse mmWave Channel Impulse Response (CIR) samples [6], while Mazzieri et al. developed Single Thresholding with Attention Refinement (STAR), a neural network-

based sparse recovery method robust to severe data loss [7]. Additionally, reinforcement learning techniques by Mason and Pegoraro intelligently schedule sensing transmissions to maximize data quality when sensing traffic is irregular [8]. Meanwhile, new datasets like dataset for integrated sensing and communication (DISC) not only facilitate further Wi-Fi sensing algorithm development by providing real 60 GHz CIR sequences of human activities in indoor environments, but can also be resampled to mimic lossy environments, thereby enabling robust algorithm testing and validation [9].

While these approaches highlight Wi-Fi sensing's potential under challenging conditions, the absence of a flexible, repeatable simulation environment remains a critical gap. Most prior efforts rely on hardware or static datasets, limiting systematic exploration and fair comparison of sensing techniques in LITSys. Addressing this gap is crucial, especially in operational military contexts requiring rigorous performance validation.

In this paper, we present an enhanced version of our open-source link-level sensing simulator, the NIST's ISAC-Physical Layer Model (PLM) framework [10]. Our extensions are tailored explicitly for IEEE 802.11bf Wi-Fi sensing research in LITSys:

1) **Extended Wi-Fi Sensing Framework**: Supporting configurable sensing timing and handling sensing packet loss, enabling the replication of real-world impairments (e.g., contention delays, packet collisions).
2) **Baseline Mitigation and Evaluation**: Implementing interpolation-based mitigation techniques as baseline solutions, quantifying performance degradation due to timing irregularities and data losses.
3) **Platform for Comparative Research**: Allowing researchers to integrate and evaluate custom algorithms under controlled conditions, enabling systematic comparisons for either synthetic or real-world measurement data.

This open simulation environment aims to accelerate Wi-Fi sensing advancements, providing researchers, including military communication system designers, with robust tools to evaluate sensing techniques in realistic, challenging operational scenarios.

The remainder of this paper is structured as follows. Section II reviews IEEE 802.11bf DMG sensing and discusses timing irregularities and packet loss implications. Section III details the ISAC-PLM framework and our new simulation extensions. Section IV presents performance results for our baseline mitigation approaches. Section V concludes the paper.

II. IEEE 802.11BF DMG SENSING AND ITS PRACTICAL CHALLENGES

A. DMG Sensing procedure in IEEE 802.11bf

In this section, we provide the necessary background on IEEE 802.11bf, with a specific emphasis on the DMG sensing procedure used for mmWave Wi-Fi sensing, as it forms the basis for the sensing measurements discussed in this paper.

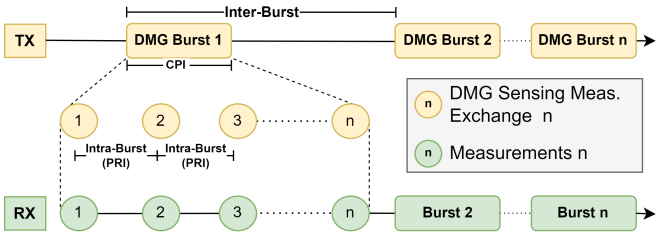

Fig. 1: IEEE 802.11bf DMG Bursts and DMG Sensing Measurement Exchange Structure

For an in-depth exploration of IEEE 802.11bf, readers are referred to [11], [12].

The IEEE 802.11bf standard introduces sensing capabilities to Wi-Fi devices, enabling stations (STAs) to advertise their sensing capabilities, establish sensing sessions, perform measurements, and report results. This paper focuses specifically on the sensing measurement process. In IEEE 802.11bf, these measurements are structured through the use of *DMG Bursts* and *DMG Sensing Measurement Exchanges*. Each DMG burst is separated by a configurable *interburst* interval, while the individual measurement exchanges within a DMG burst are spaced by a configurable *intraburst* interval, as illustrated in Fig. 1. These DMG Sensing Measurement Exchanges act as discrete sensing points used for sensing processing. A single DMG burst consists of n such measurements.

From a radar perspective, the intraburst interval corresponds to the Pulse Repetition Interval (PRI), while the overall duration of the burst maps to the Coherent Processing Interval (CPI). The collection of these measurements enables sensing operations, including, but not limited to Range-Doppler (RD) processing. The structure and periodicity of DMG bursts determine the temporal resolution of the sensing system, effectively acting as the tracking frequency, and make it possible to extract features such as micro-Doppler signatures. For readers interested in radar signal processing in the context of IEEE 802.11bf, we refer to [13].

DMG sensing measurement exchanges are carried out through the transmission of specific PHY Protocol Data Units (PPDUs), with the format depending on the sensing configuration (i.e., monostatic, bistatic, or multistatic). This paper focuses on the bistatic scenario, where a dedicated sensing transmitter sends frames that are received and processed by a separate receiver. This setup is particularly attractive for military applications, as a high-powered central device can effectively communicate with strategically deployed, battery-operated receivers to ensure broad and flexible coverage of the operational field.

In a bistatic configuration, measurements use Beam Refinement Protocol (BRP) PPDUs with appended Trainings (TRNs) fields. First introduced in IEEE 802.11ad and retained in 802.11ay, these TRN sequences, thanks to their strong autocorrelation, enable precise channel estimation and fine-grained sensing.

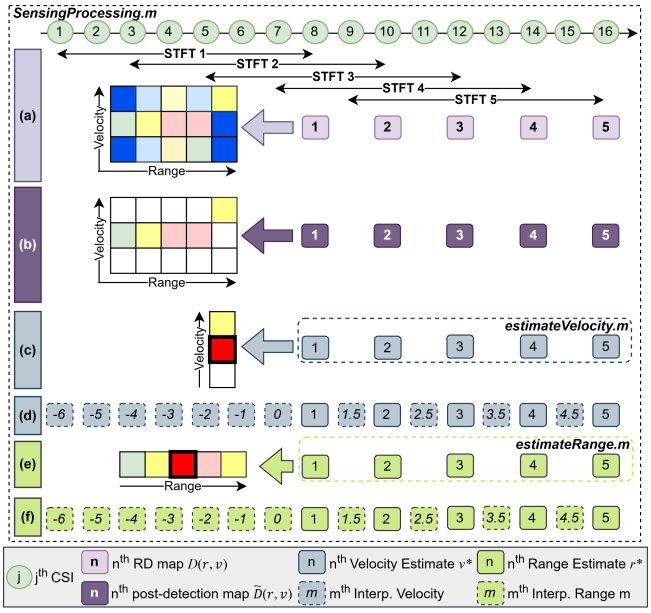

Fig. 2: Overview of ISAC-PLM sensing processing module. (a) RD Maps Processing. (b) Peak detection (c) Velocity estimation (Data are aggregated over the range bins) (d) Velocity interpolation (e) Range estimation (Data are aggregated over the velocity bins) (f) Range interpolation.

B. Limitations of Wi-Fi for Reliable Sensing

Performing reliable sensing in Wi-Fi networks presents inherent challenges. At the device level, Wi-Fi is and will remain a communication protocol first, unlike dedicated radar systems, which rely on deterministic waveforms and scheduled transmissions. IEEE 802.11bf enables sensing through the use of dedicated sensing PPDUs, and these transmissions must compete with the station's own communication traffic. Depending on how sensing traffic is queued relative to ongoing communication flows, additional delays may be introduced. At a broader scale, Wi-Fi operates under a best-effort, contention-based medium access model. This means that sensing traffic, like all other traffic, must contend for access to the wireless medium. When surrounding data traffic is present, sensing inherits the associated irregularities, delays, and potential packet losses. These characteristics make Wi-Fi sensing a representative example of a LITSys.

In IEEE 802.11bf DMG sensing, each DMG sensing measurement exchange requires explicit channel access. Medium access in Wi-Fi is governed by the Carrier Sense Multiple Access with Collision Avoidance (CSMA/CA) protocol, which employs contention windows and random backoff timers to resolve conflicts. This mechanism leads to non-deterministic transmission intervals, severely degrading temporal coherence, an essential requirement for Doppler and micro-Doppler processing. In dense environments or scenarios with hidden terminals and interference (e.g., urban combat zones with obstructed lines of sight and unpredictable RF conditions), packet collisions and frame losses further increase measurement sparsity and timing irregularity. These issues are amplified in mmWave Wi-Fi systems due to the propagation characteristics of high-frequency signals. mmWave links are highly directional and vulnerable to beam misalignment, blockage by moving objects, and rapid signal attenuation. Even line-of-sight links can experience intermittent dropouts, resulting in unpredictable gaps in measurement sequences.

Collectively, these factors make IEEE 802.11-based mmWave sensing inherently lossy and temporally irregular, fundamentally diverging from the deterministic assumptions of traditional radar systems. To facilitate evaluation under these non-deterministic conditions, we extend the ISAC-PLM framework with configurable impairments, as detailed in the next section.

III. ISAC-PLM Framework with Irregular Timing and Packet Loss

A. Standard ISAC-PLM Framework

The ISAC-PLM framework[1] is a MATLAB-based open-source link-level simulation platform for ISAC systems, focusing on mmWave Wi-Fi sensing compliant with IEEE 802.11bf standards. It integrates a full IEEE 802.11ay transceiver and a sensing module. Configuration files allow users to set PHY parameters (e.g., PPDU/TRN settings), sensing parameters (e.g., Doppler processing), and the channel model, a JSON file containing multipath components (MPCs) with their delays, phases, AOAs, and AODs. The framework can support any channel generator or real-world dataset (e.g., DISC) as long as the channel provided respect the JSON expected format.

For every simulated transmission, ISAC-PLM uses the IEEE 802.11ay baseband chain to modulate sensing-specific PPDU frames, simulate propagation through a time-varying multipath environment, and extract Channel State Information (CSI) from the Channel Estimation Field (CEF) segment of each packet. The sensing module then enables the construction of a three-dimensional data cube (range–angle–time) from sequential CSI measurements and generates radar outputs such as RD maps, range–angle maps, and micro-Doppler signatures. Doppler information is extracted using the Short-time Fourier transform (STFT), with configurable parameters including the window length, overlap, and fast Fourier transform (FFT) size. Fig. 2a illustrates the generation of RD maps using a window length of 8 and an overlap of 0.8, resulting in five distinct maps. While the angular dimension is not shown in the figure, ISAC-PLM fully supports beamforming. When beamforming is enabled, an additional angular dimension is introduced, and Fig. 2 can be interpreted as a slice corresponding to a specific beam.

After obtaining the raw range–Doppler maps $D(r, v)$ (where r represents range bins and v represents Doppler bins) the sensing module enables peak detection as depicted in

[1] Available online: https://github.com/wigig-tools/isac-plm

Fig. 2b, using either 2D-constant false alarm rate (CFAR) or a custom dedicated peak-finding algorithm. The resulting post-detection map, denoted by $\tilde{D}(r, v)$, is aggregated over the angular domain to yield a one-dimensional profile for further processing.

Subsequently, velocity and range estimates are detected from $\tilde{D}(r, v)$ using the routines `estimateVelocity.m` and `estimateRange.m` (Fig. 2c and Fig. 2e). The range profile is given by $R(r) = \sum_v |\tilde{D}(r, v)|$ and the range estimate is determined by $r^* = \arg\max_r R(r)$. Similarly, the velocity profile is $V(v) = \sum_r |\tilde{D}(r, v)|$ with $v^* = \arg\max_v V(v)$. In practice, ISAC-PLM offers several detection methods.

Interpolation and extrapolation may optionally be applied to generate additional estimates between detected values (Fig. 2d and Fig. 2f). For range, linear interpolation (with extrapolation at the boundaries) is used to fill gaps between available detections. Similarly, velocity estimates are refined using linear interpolation followed by low-pass filtering (LPF) to suppress high-frequency noise, with the LPF bandwidth adjustable according to the application's expected velocity.

B. Enhancements for LITSys

We have extended ISAC-PLM to effectively support LITSys. Timing irregularities and packet losses are explicitly modeled through the `sensingTiming.csv` file, where each row specifies the exact timestamp of a DMG sensing measurement exchange within a given DMG burst. Missing measurements are represented by omission, accurately reflecting real-world impairments such as network-induced delays and packet drops.

To handle LITSys, ISAC-PLM reconstructs uniformly sampled CSI from sparse measurements using the module `recoverSparseCsi.m`. For each delay bin d and angular channel a, denote the available CSI measurements as $H(d, m, a)$ for $m = 1, \ldots, M$, acquired at irregular times $\{t_m\}_{m=1}^{M}$. We wish to reconstruct a uniformly sampled CSI representation at times

$$\tau_n = (n-1)T_{\mathrm{PRI}}, \quad n = 1, \ldots, N.$$

where T_{PRI} is the pulse repetition interval and N is the number of pulses per burst. If there is no measurement at a desired time τ_n (i.e., a missed measurement due to irregular timing or packet loss), we identify the two adjacent indices m_1 and m_2 such that

$$t_{m_1} \leq \tau_n \leq t_{m_2}.$$

Then, the missing CSI is estimated by linear interpolation:

$$\hat{H}(d, n, a) = H(d, m_1, a) + \frac{H(d, m_2, a) - H(d, m_1, a)}{t_{m_2} - t_{m_1}} (\tau_n - t_{m_1}).$$

Boundary cases (where τ_n lies outside the range of available t_m) are handled by extrapolation. This procedure yields a reconstructed CSI $\hat{H}(d, n, a)$ that is continuously and uniformly sampled for subsequent sensing analysis. This serves as a baseline implementation of a sparse recovery. Researchers seeking to explore alternative CSI reconstruction techniques can easily implement and evaluate their methods within ISAC-PLM by modifying or extending the `recoverSparseCsi.m` module.

IV. Performance Evaluation Case Study

This section illustrates the capabilities of our ISAC-PLM framework in managing LITSys, using a realistic scenario representing a surveillance setup of a forward-deployed military outpost or a temporary command center.

A. Scenario Description and parameters

The monitored environment is a room measuring 7 m $\times$ 7 m $\times$ 3 m, containing a single human target following a predefined trajectory modeled via Boulic motion [14]. Boulic motion effectively replicates human walking dynamics by simulating articulated joint kinematics [15]. The wireless channel is implemented using the NIST quasi-deterministic (QD) Channel Realization Software[2], which provides realistic double-directional CIRs through 3D ray-tracing combined with statistical modeling.

The objective is real-time intrusion detection and situational awareness by estimating target range and velocity. We operate in the 60 GHz mmWave band with 2 GHz bandwidth using IEEE 802.11bf, achieving high range resolution ($\approx$ 7.5 cm). To simplify the analysis, ISAC-PLM is configured to transmit omnidirectionally. However, the results remain applicable when employing phased antenna arrays (PAAs) for beamformed communication. The setup is bistatic, with the transmitter and receiver positioned opposite each other on the ceiling. Each scenario uses 10 DMG bursts of 64 BRP exchanges. We apply an STFT with a 16-sample window and 0.8 overlap, generating 65 RD maps, and thus 65 velocity and range estimates, per scenario, using an FFT size of 64.

Using the IEEE TGbf use-case document [16], which lists sensing-accuracy requirements for applications such as gesture recognition and healthcare, we selected the presence–detection profile as our baseline: velocity accuracy of 0.1 m/s, maximum observable velocity of 2 m/s, and range accuracy of 50 cm. By radar principles, these translate to an intraburst interval $\mu = 625$ μs and an interburst interval $\tau = 100$ ms. These timing parameters, combined with our chosen FFT size, yield a velocity resolution of 0.06 m/s.

For timing and loss modeling, each DMG burst initiates at time $B_k = B_1 + (k-1)\tau$, where B_1 is the time of the first burst, τ is the interburst interval, and $k = 1, 2, \ldots$. Within each burst, the nominal time for the i-th DMG sensing measurement exchange (with $n = 64$) is given by $T_{k,i} = B_k + (i-1)\mu$ where μ is the intraburst interval. We model the additional jitter due to irregular Wi-Fi timing for each intraburst interval ($i \geq 2$) as

$$\Delta t_{k,i} = \mu + \max\{\epsilon_{k,i}, 0\}, \quad \epsilon_{k,i} \sim \mathcal{N}(0, \sigma^2),$$

[2]Available online: https://github.com/wigig-tools/qd-realization

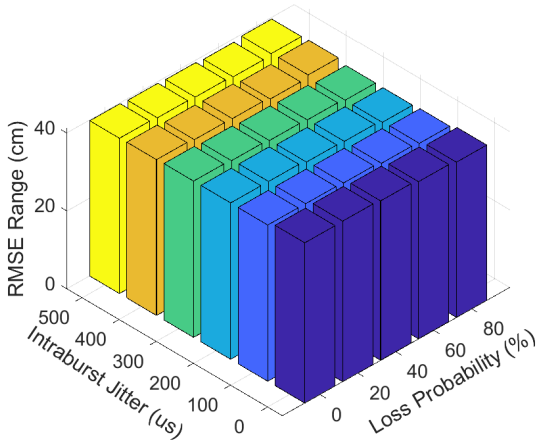

Fig. 3: Effect of packet loss and intraburst jitter on RMSE range across all scenarios and seeds.

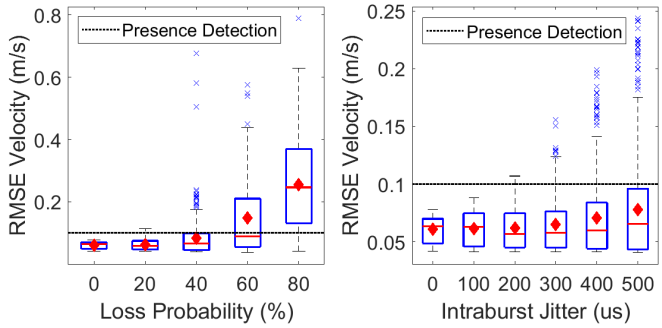

(a) RMSE Velocity vs. Packet Loss.

(b) RMSE Velocity vs. Intraburst Jitter.

Fig. 4: Effect of packet loss and intraburst jitter on RMSE velocity across all scenarios and seeds.

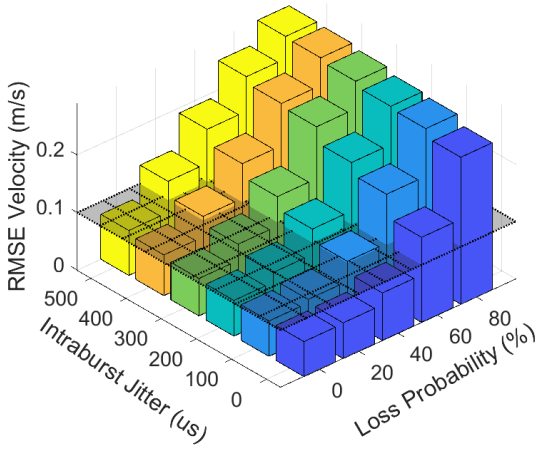

Fig. 5: Effect of packet loss and intraburst jitter on the velocity RMSE across all scenarios and seeds. The black transparent mesh represents the 0.1 m/s velocity accuracy threshold required for presence detection.

ensuring that only positive delays occur (i.e., packets cannot arrive earlier than scheduled). Independently, each measurement is dropped with probability p to emulate network congestion. To avoid burst overlap (a measurement belonging to a DMG burst cannot be sent after a subsequent burst was started), we set $\sigma = 500\ \mu$s[3].

We systematically vary σ from 0 to 500 μs in increments of 100 μs and the packet loss rate p from $0\,\%$ to $80\,\%$ in increments of $20\,\%$. For statistical robustness, results are averaged over 30 distinct seeds (affecting drop timing and jitter) and 30 different initial positions and trajectories for the human subject, yielding 900 simulations per intraburst jitter/packet loss rate combination.

We assess the sensing performance using the Root Mean Squared Error (RMSE) of the velocity and the range, defined as RMSE $= \sqrt{\frac{1}{N}\sum_{j=1}^{N}(\hat{x}_j - x_j)^2}$, where $\hat{x}_j$ are the estimated measurements and x_j are the ground truth values, computed from the collected RD maps. We report average RMSE across all timing seeds and scenarios for a comprehensive performance summary. To isolate direct RD map estimates, we disable the optional interpolation between real estimates (Sec.III-A, Fig.2d,f). Under LITSys, we enable the interpolation from Section III-B to reconstruct uniformly sampled CSI despite delayed or missing measurements.

B. Evaluation Results

Fig. 3 illustrates the range estimation RMSE as a function of packet losses and intraburst jitter. We can see that the range RMSE remains consistently low at approximately 40 cm, irrespective of the intraburst jitter or the extent of packet losses. This robust performance is primarily due to the high range resolution achievable with mmWave systems, which ensures that the performance meets the 50 cm requirement for presence detection. Moreover, the stability in range estimation is inherently related to the measurement process. Unlike velocity estimation, which necessitates Doppler processing, a single measurement is sufficient to estimate range when the signal-to-noise ratio is adequate. Consequently, missing or irregular packets do not substantially affect the overall range estimation performance, as additional measurements primarily provide an integration gain that refines the estimate. The intrinsic stability of the range measurements for human targets over the sampling duration, combined with the interpolation of the CSI presented in Section III-B, explains the consistently favorable results across varying parameters.

For velocity estimation, Fig. 4a and 4b show the velocity RMSE for packet loss or intraburst jitter alone, demonstrating that both degrade accuracy. Unlike range estimation, velocity extraction via Doppler processing with the STFT requires phase continuity across multiple measurements; irregular intervals and lost packets break this coherence, causing spectral leakage and aliasing. Although linear interpolation methods

[3]We did not consider interburst jitter, although it can indeed occur. Our primary goal was to demonstrate the need for an open-source platform capable of handling LITSys. Therefore, we opted for a low-dimensional scenario that remains highly interpretable.

are used to reconstruct CSI missing samples, these baseline techniques cannot fully restore the phase coherence necessary for accurate velocity estimation. This degradation complicates peak detection and results in elevated velocity RMSE values, underscoring the importance of the LITSys study and the need for sparse recovery methods and frameworks for comprehensive algorithm evaluation. We can additionnaly observe that the packet losses have a substantially greater impact on velocity accuracy than intraburst jitter. For example, at an 80 % packet loss, the median velocity RMSE reaches approximately 0.25 m/s, whereas with a maximum intraburst jitter of 500 μs, the median RMSE remains around 0.07 m/s. This is because each lost packet creates an unrecoverable phase gap in the STFT window sequence, causing severe spectral leakage, whereas moderate timing offsets simply shift sample instants by small amounts that interpolation can largely correct.

Considering the presence detection requirement of 0.1 m/s, the average velocity RMSE (represented by the diamond markers) exceeds this threshold when packet loss surpasses 40 %. In contrast, regardless of the intraburst jitter values, at least 75 % of the measurements (as indicated by the upper quartile of the boxplot) remain below the desired velocity accuracy and all the median values are below 0.1 m/s.

Finally, the comprehensive 3D analysis in Fig. 5, which simultaneously varies both intraburst jitter and packet loss, clearly shows that the presence detection velocity requirement of 0.1 m/s is violated when packet loss exceeds 40 % or when 40 % packet loss occurs in combination with any nonzero intraburst jitter, with performance further degrading as jitter increases (notably, at the maximum intraburst jitter of 500 μs, the velocity requirement is always exceeded as soon as any packet loss occurs).

These findings underscore the importance of robust frameworks capable of handling such impairments, particularly in tactical or military applications. Our enhanced ISAC-PLM framework provides a valuable open-source platform for exploring, evaluating, and optimizing integrated sensing and communication systems under realistic conditions.

V. Conclusion

In this paper, we introduced significant enhancements to the ISAC-PLM open-source simulation framework tailored to IEEE 802.11bf mmWave sensing, explicitly addressing practical conditions involving irregular timing and packet loss. By modeling realistic impairments that arise in contested, congested, and dynamically changing wireless environments, our platform enables comprehensive and reproducible evaluation of sensing algorithm performance. Simulations of a military-relevant indoor surveillance scenario show that range estimation remains robust under severe packet loss, while velocity estimation degrades significantly with packet loss and, to a lesser extent, with intraburst jitter. These results emphasize the importance of developing advanced resilient sensing techniques, especially in adversarial or operationally challenging scenarios. The proposed extended ISAC-PLM framework fills a critical gap in Wi-Fi sensing research, providing a necessary foundation for future investigations into robust sensing methodologies under realistic conditions.

As future work, we plan to leverage system-level simulators such as ns-3 to evaluate the end-to-end performance of IEEE 802.11bf under realistic conditions. This approach will account for cross-layer interactions and surrounding traffic, enabling accurate characterization of intraburst and interburst jitters as well as sensing-related packet losses.

References

[1] S. Mandelli, M. Henninger, M. Bauhofer, and T. Wild, "Survey on integrated sensing and communication performance modeling and use cases feasibility," in *2023 2nd International Conference on 6G Networking (6GNet)*, pp. 1–8, 2023.

[2] "IEEE P802.11bf™/D6.0 Draft Standard for Information technology—Telecommunications and information exchange between systems Local and metropolitan area networks— Specific requirements Part 11: Wireless LAN Medium Access Control (MAC) and Physical Layer (PHY) Specifications Amendment 2: Enhancements for Wireless LAN Sensing," 2024.

[3] A. Sahoo, T. Ropitault, S. Blandino, and N. Golmie, "Sensing performance of the IEEE 802.11bf protocol and its impact on data communication," in *2024 IEEE 100th Vehicular Technology Conference (VTC2024-Fall)*, pp. 1–7, 2024.

[4] D. Donoho, "Compressed sensing," *IEEE Transactions on Information Theory*, vol. 52, no. 4, pp. 1289–1306, 2006.

[5] E. Crespo Marques, N. Maciel, L. Naviner, H. Cai, and J. Yang, "A review of sparse recovery algorithms," *IEEE Access*, vol. 7, pp. 1300–1322, 2019.

[6] J. Pegoraro, J. O. Lacruz, M. Rossi, and J. Widmer, "SPARCS: A sparse recovery approach for integrated communication and human sensing in mmWave systems," in *2022 21st ACM/IEEE International Conference on Information Processing in Sensor Networks (IPSN)*, pp. 79–91, 2022.

[7] R. Mazzieri, J. Pegoraro, and M. Rossi, "Attention-refined unrolling for sparse sequential micro-doppler reconstruction," *IEEE Journal of Selected Topics in Signal Processing*, vol. 18, no. 5, pp. 812–827, 2024.

[8] F. Mason and J. Pegoraro, "Using deep reinforcement learning to enhance channel sampling patterns in integrated sensing and communication," *IEEE Wireless Communications Letters*, vol. 14, no. 3, pp. 821–825, 2025.

[9] J. Pegoraro, P. Saucedo, J. O. Lacruz Jucht, M. Rossi, and J. Widmer, "DISC: a dataset for integrated sensing and communication in mmWave systems," 2022.

[10] S. Blandino, N. Varshney, J. Wang, and J. Zhang, "Integrated Sensing and Communication Physical Layer Model (ISAC-PLM)," 2025. National Institute of Standards and Technology (NIST).

[11] T. Ropitault, C. R. C. M. da Silva, S. Blandino, A. Sahoo, N. Golmie, K. Yoon, C. Aldana, and C. Hu, "IEEE 802.11bf WLAN sensing procedure: Enabling the widespread adoption of WiFi sensing," *IEEE Communications Standards Magazine*, vol. 8, no. 1, pp. 58–64, 2024.

[12] R. Du, H. Hua, H. Xie, X. Song, Z. Lyu, M. Hu, Narengerile, Y. Xin, S. McCann, M. Montemurro, T. X. Han, and J. Xu, "An overview on IEEE 802.11bf: WLAN sensing," *IEEE Communications Surveys and Tutorials*, pp. 1–1, 2024.

[13] S. Blandino, T. Ropitault, C. R. C. M. da Silva, A. Sahoo, and N. Golmie, "IEEE 802.11bf DMG sensing: Enabling high-resolution mmWave Wi-Fi sensing," *IEEE Open Journal of Vehicular Technology*, vol. 4, pp. 342–355, 2023.

[14] R. Boulic, N. M. Thalmann, and D. Thalmann, "A global human walking model with real-time kinematic personification," *The visual computer*, vol. 6, no. 6, pp. 344–358, 1990.

[15] S. Blandino, T. Ropitault, A. Sahoo, and N. Golmie, "Tools, models and dataset for IEEE 802.11ay CSI-based sensing," in *2022 IEEE Wireless Communications and Networking Conference (WCNC)*, pp. 662–667, 2022.

[16] "TGbf Evaluation Methodology and Simulation Scenarios Document," 2023. Document 11-21/0876r5, Last update: January 2023.